sciendo

POLISH MARITIME RESEARCH 2 (102) 2019 Vol. 26; pp. 198-211
10.2478/pomr-2019-0039

THE PREDICTION OF HULL GESTURE AND FLOW AROUND SHIP BASED ON TAYLOR EXPANSION BOUNDARY ELEMENT METHOD

Jiaye Gong
College of Shipbuilding Engineering, Harbin Engineering University, Harbin, China
Yunbo Li
College of Ocean Science and Engineering of SMU, Shanghai Maritime University, Shanghai, China

ABSTRACT

Based on the potential flow theory and traditional boundary element method (BEM), Taylor expansion boundary element method (TEBEM) is introduced in this paper for the prediction of the flow field around ship, as a result, hull gesture and pressure distribution on hull surface are obtained. By this method, dipole strength of every field point is expanded in Taylor expansion, so that approximately continuous hull and free surface boundary condition could be achieved. To close the new equation system, the boundary condition of tangent velocity in every control point is introduced. With the simultaneous solving of hull boundary condition and free surface condition, the disturbance velocity potential could be obtained. The present method is used to predict the flow field and hull gesture of Wigley parabolic hull, Series 60 and KVLCC2 models. To validate the numerical model for full form ship, the wave profile, the computed hull gesture and hull surface pressure of KVLCC2 model are compared with experimental results.

Keywords: TEBEM, potential flow, flow field, hull gesture, surface pressure

INTRODUCTION

In ship hydrodynamics, prediction of flow around ship and hull gesture in calm water is a fundamental problem, and a high degree of numerical calculation precision and efficiency is required for ship design [24]. Based on the viscous flow theory, there has been used some commercial software to predict accurately the resistance of ship hull, but a large number of numerical iterations in a big spatial computational domain is necessary, which is time-consuming and limiting its application for practical design and hull form optimization [25, 26], especially in case of a large-scale model. For some problems less affected by fluid viscosity, such as the wave profile and ship hull gesture [17], the potential flow theory is still an effective method to solve the problems.

For potential flow methods, Dawson's method [3] is still a very effective and popular method for the prediction of wave-making resistance, because both pressure distribution on hull surface and the near-field flow can be predicted by this method. But, for the limitation of the streamline mesh and difference, the original Dawson's method is not accurate enough. Rapid method [15, 16] is proposed to solve the fully non-linear wave-making problem. By numerical iteration of the free surface, wave profile and pressure distribution along hull surface could be obtained, and the result is precise and close to the experimental result. By large amount of experiments and regression analysis, the numerical prediction method is improved for wave-making resistance of ships with transom-stern [4, 5]. The empirical formula obtained from experiments is used to predict the ventilation length and depth behind transom-stern, and the result is in good agreement with the experimental result. The Dawson's method is improved and the numerical method is optimized [21]. The improved method is used to predict the wave-making resistance of fixed ship hull. Based on the boundary element method (BEM), panels are arranged on the bottom to predict the wave-making resistance of a catamaran at a finite water depth [22]. The wave-making resistance of a pentamaran is

predicted at infinite depth of water by using the BEM and the linearized free surface condition with second order terms [19], and the Froude number up to 0.8. Linear wave-making theory is applied to determine the bow bulbs and hull form for full body ship with the minimum total resistance [25, 26].

In nowadays marine industry, full form ships still play a main role in passenger and freight service, such as commercial bulk carriers and container ships with block coefficient larger than 0.6 and 0.8 , respectively. In recent years, with the Energy Efficiency Design Index (EEDI) introduced by IMO, the demand for improved cargo capacity, fuel efficiency, low emissions and optimized operation is more and more important during the process of ship design and optimization [9, 12], and it also influences the design and the selection of operational profile with emphasis on low speed service. Consequently, most of the research about hull form optimization of full body ship is carried out for bulk carriers, container ships and oil tankers with low design speed [11, 18]. Compared with a high-speed slim ship, the prediction of flow field and hull gesture is more complex for ships with full hull form with low speed [14], because the surface curvature of full form ship is relatively larger in stem and stern areas, and the numerical solution is usually not stable in the areas as oscillation of the wave profile usually occurs. Therefore, it is meaningful to improve the numerical method to predict efficiently and stably the flow field and hull gesture of ships with large block coefficient and low speed.

In 2012, by expanding dipole potential in Taylor expansion, the 2-D TEBEM was proposed [6]. This way the precision of the tangential velocity could be improved in the non-smooth boundary. If the first-order derivative is kept, it is called the first-order TEBEM. If the second-order derivative is kept, it is called the second-order TEBEM. By combining the first-order TEBEM and the second-order TEBEM, the TEBEM method is applied to solve 3-D hydrodynamic characteristics of ship with forward speed [1], and the calculated result is in good agreement with the experimental one.

In this paper, the TEBEM is combined with linear wave-making theory to predict the wave-making resistance and hull gesture. The expansion of dipole potential will lead to a non-closed equation system, whereas the derivation of a complementary equation is completed. The convergence of the method is tested, and its application to different hull forms is analyzed. By numerical simulation of different hull forms, the numerical results of wave making resistance, hull gesture, wave profile and hull surface pressure are compared with the experimental result to validate the accuracy of this method.

METHODS

The TEBEM is firstly introduced into the numerical simulation of flow and hull gesture. Because of the expansion of dipole strength in Taylor expansion, the derivation of the new boundary condition is discussed in this section.

BASIC EQUATION

The coordinate system is fixed to ship hull, and its origin is in an undisturbed free surface amidships. The x-axis and y-axis extend to stern and starboard respectively. A ship is advancing at a constant speed U along the positive direction of x-axis.

It is assumed that the fluid is ideal, the flow around the ship is constant, and the water depth is infinite. Φ is defined as the total velocity potential which satisfies Laplace equation:

$$\nabla^2 \Phi = 0 \tag{1}$$

The total velocity potential Φ is divided into the double-body flow velocity potential ϕ and the perturbed velocity potential φ, where φ represents the interaction between ship hull and the free surface:

$$\Phi = \phi + \varphi \tag{2}$$

$$\zeta = \xi + \eta \tag{3}$$

where ζ, ξ and η are the wave profile corresponding to total velocity potential Φ, double-body flow velocity potential ϕ and perturbed velocity potential φ.

The double-body flow velocity potential ϕ is subdivided into the velocity potential of incoming flow potential and velocity potential $\overline{\varphi}$, which represents the perturbation by the double-body:

$$\phi = Ux + \overline{\varphi} \tag{4}$$

Because the velocity potential of incoming flow is included in the double-body flow potential, the perturbed velocity potential φ is assumed much lower than double-body velocity potential ϕ. The corresponding wave profile follows the similar assumption:

$$\varphi << \phi \quad \eta << \xi \tag{5}$$

HULL SURFACE BOUNDARY CONDITION

The normal velocity components of both the double-body potential ϕ and the perturbed potential φ are zero on the hull surface:

$$\nabla \overline{\varphi} \cdot \boldsymbol{n} = -\boldsymbol{U} \cdot \boldsymbol{n} \tag{6}$$

$$\nabla \varphi = 0 \tag{7}$$

Where $\boldsymbol{n}$ is specified as the normal vector of the hull surface.

FREE SURFACE CONDITION

The total velocity potential Φ satisfies both the kinematic condition and dynamic condition on the free surface:

$$\Phi_x\zeta_x + \Phi_y\zeta_y - \Phi_z = 0 \qquad z = \zeta \tag{8}$$

$$g\zeta + \frac{1}{2}(\nabla\Phi\cdot\nabla\Phi - U^2) = 0 \qquad z = \zeta \tag{9}$$

We eliminate the ζ from simultaneous Eqs. (8) and (9) to obtain the free surface condition

$$\nabla\Phi\nabla\left[\frac{1}{2}(\nabla\Phi\nabla\Phi)\right] + g\Phi_z = 0 \quad z = \zeta \tag{10}$$

We insert Eqs. (1) to Eqs. (10) to get the total velocity potential Φ expanded in Taylor expansion about $z = \xi$ and $z = 0$ respectively. The nonlinear term of φ is neglected to obtain linearized free surface condition:

$$\frac{1}{2}\phi\,(\phi_x^2+\phi_y^2)_x + \frac{1}{2}\phi_y(\phi_x^2+\phi_y^2)_y + \phi_x(\phi_x\varphi_x+\phi_y\varphi_y)_x + \phi_y(\phi_x\varphi_x+\phi_y\varphi_y)_y$$
$$+\frac{1}{2}\varphi_x(\phi_x^2+\phi_y^2)_x + \frac{1}{2}\varphi_y(\phi_x^2+\phi_y^2)_y + g\varphi_z = 0 \qquad z=0 \tag{11}$$

Because $\varphi << \phi$, it is assumed that:

$$\varphi_x + \varphi_y = \varphi_l \tag{12}$$

where the subscript l represents the derivation along streamline of double-body flow ϕ.

The free surface condition is obtained as follows:

$$2\phi_l\phi_{ll}\varphi_l + \phi_l^2\varphi_{ll} + g\varphi_z = -\phi_l{}^2\phi_{ll} \quad z = 0 \tag{13}$$

The radiation condition is also satisfied on the free surface. Based on the investigation by Nakos [13], the truncation error of the upstream free surface will significantly affect the simulation result. So, to make the radiation condition satisfied, an upstream finite difference scheme [3, 21] is applied to make sure that the flow propagates downstream, and the boundary conditions $\varphi_x = U$ and $\varphi_y = 0$ are used in the upstream panels far from the ship by means of virtual panels.

APPLICATION OF THE TEBEM

Laplace equation is transformed to integral form:

$$4\pi\bar{\varphi} = -\iint_{S_B}\frac{\partial}{\partial n}(\frac{1}{r})\bar{\varphi}dS + \iint_{S_B}(\frac{1}{r})(\frac{\partial\bar{\varphi}}{\partial n})dS \tag{14}$$

The double-body velocity potential in i-th panel of hull surface is specified as $\bar{\varphi}(i)$. Eqs. (14) is discretized and expressed as:

$$4\pi\bar{\varphi}(i) = -\sum_{j=1}^{N_B}\iint_{S_B}\frac{\partial}{\partial n_j}(\frac{1}{r_{ij}})\bar{\varphi}(j)dS_j + \sum_{j=1}^{N_B}\iint_{S_B}(\frac{1}{r_{ij}})(\frac{\partial\bar{\varphi}(j)}{\partial n_j})dS_j \tag{15}$$

where r_{ij} is the distance between i-th field point and j-th source point.

In the right side of Eqs. (15), the first term is the dipole model, and the second term is the source model. (x', y', z') is specified as the local co-ordinate system of source panel. The dipole density $\bar{\varphi}(j)$ of j-th panel is expanded in Taylor expansion in the local co-ordinate system, and the first order of $\bar{\varphi}(j)$ is kept:

$$\bar{\varphi}(j) = \bar{\varphi}(j_0) + \frac{\partial\bar{\varphi}(j_0)}{\partial x'}x' + \frac{\partial\bar{\varphi}(j_0)}{\partial y'}y' \tag{16}$$

where j_0 represents the origin of j-th panel.

After inserting Eqs. (16) to Eqs. (15), the discretized Eqs. (15) can be expressed as:

$$4\pi\bar{\varphi}(i) + \sum_{j=1}^{N_B}\iint_{S_B}\frac{\partial}{\partial n_j}(\frac{1}{r_{ij}})\bar{\varphi}(j)dS + \sum_{j=1}^{N_B}\iint_{S_B}\frac{\partial}{\partial n_j}(\frac{1}{r_{ij}})\bar{\varphi}_{x'}(j)x'dS_j$$
$$+\sum_{j=1}^{N_B}\iint_{S_B}\frac{\partial}{\partial n_j}(\frac{1}{r_{ij}})\bar{\varphi}_{y'}(j)y'dS_j$$
$$= -\sum_{j=1}^{N_B}\iint_{S_B}(\frac{1}{r_{ij}})(\boldsymbol{U}\cdot\boldsymbol{n}_j)dS_j \tag{17}$$

where $i = 1, 2..., N_b$

In Eqs. (17), the double-body flow velocity potential and its tangential derivatives are the unknown numbers to be determined. For 3-D problem, if the hull surface is discretized into N panels, there are $3N$ unknown numbers to be found. Hence, we should introduce $2N$ equations to complete the equation system.

We specify (x, y, z) as the co-ordinate system of i-th field panel, introduce the tangential derivation of Eqs. (17) along the x-axis and y-axis, and the complete equation system is obtained:

$$4\pi(\bar{\varphi})_i + \sum_{j=1}^{N_b}D_{ij}(\bar{\varphi})_j + \sum_{j=1}^{N_b}(D^{x'})_{ij}(\bar{\varphi}_{x'})_j + \sum_{j=1}^{N_b}(D^{y'})_{ij}(\bar{\varphi}_{y'})_j = -\sum_{j=1}^{N_b}S_{ij}(\boldsymbol{U}\cdot\boldsymbol{n}_j) \tag{18}$$

$$4\pi(\bar{\varphi}_x)_i + \sum_{j=1}^{N_b}(D_x)_{ij}(\bar{\varphi})_j + \sum_{j=1}^{N_b}(D_x^{x'})_{ij}(\bar{\varphi}_{x'})_j + \sum_{j=1}^{N_b}(D_x^{y'})_{ij}(\bar{\varphi}_{y'})_j = -\sum_{j=1}^{N_b}(S_x)_{ij}(\boldsymbol{U}\cdot\boldsymbol{n}_j) \tag{19}$$

$$4\pi(\bar{\varphi}_y)_i + \sum_{j=1}^{N_b}(D_y)_{ij}(\bar{\varphi})_j + \sum_{j=1}^{N_b}(D_y^{x'})_{ij}(\bar{\varphi}_{x'})_j + \sum_{j=1}^{N_b}(D_y^{y'})_{ij}(\bar{\varphi}_{y'})_j = -\sum_{j=1}^{N_b}(S_y)_{ij}(\boldsymbol{U}\cdot\boldsymbol{n}_j) \tag{20}$$

where

$$D_{ij}=\iint_{Sb_j}\frac{\partial}{\partial n_j}\left(\frac{1}{r_{ij}}\right)ds_j \quad (D^{x'})_{ij}=\iint_{Sb_j}x'\frac{\partial}{\partial n_j}\left(\frac{1}{r_{ij}}\right)ds_j \quad (D^{y'})_{ij}=\iint_{Sb_j}y'\frac{\partial}{\partial n_{ij}}\left(\frac{1}{r_{ij}}\right)ds_j \quad S_{ij}=\iint_{Sb_j}\frac{1}{r_{ij}}ds_j$$

$$(D_x)_{ij}=\iint_{Sb_j}\frac{\partial}{\partial x}\left(\frac{1}{r_{ij}}\right)ds_j \quad (D_x^{x'})_{ij}=\iint_{Sb_j}x'\frac{\partial}{\partial x}\left(\frac{1}{r_{ij}}\right)ds_j \quad (D_x^{y'})_{ij}=\iint_{Sb_j}y'\frac{\partial}{\partial x}\left(\frac{1}{r_{ij}}\right)ds_j \quad (S_x)_{ij}=\iint_{Sb_j}\frac{\partial}{\partial x}\left(\frac{1}{r_{ij}}\right)ds_j$$

$$(D_y)_{ij}=\iint_{Sb_j}\frac{\partial}{\partial y}\left(\frac{1}{r_{ij}}\right)ds_j \quad (D_y^{x'})_{ij}=\iint_{Sb_j}x'\frac{\partial}{\partial y}\left(\frac{1}{r_{ij}}\right)ds_j \quad (D_y^{y'})_{ij}=\iint_{Sb_j}y'\frac{\partial}{\partial y}\left(\frac{1}{r_{ij}}\right)ds_j \quad (S_y)_{ij}=\iint_{Sb_j}\frac{\partial}{\partial y}\left(\frac{1}{r_{ij}}\right)ds_j$$

Consequently, the amount of the equations is equal to the amount of the unknown numbers. The double-body flow velocity potential $\overline{\varphi}$ and its derivatives $\overline{\varphi}_{x'}$ and $\overline{\varphi}_{y'}$ are obtained by solving the linear system from Eqs. (18) to (20).

The integration procedure of the coefficients in Eqs. (18) to (20) is similar to the Hess-Smith approach [2], which is estimated in the local coordinate system of the panel S_j. The centre of local coordinate system is the geometric centre of the panel S_j. If we take D_{ij}, $(D_x)_{ij}$ and $(D_y)_{ij}$ for example, the integration can be expressed as

$$D_{ij}=\sum_{k=1}^{N}(\arctan\frac{m_{k,k+1}c_k-h_k}{z'_i\,r_k}-\arctan\frac{m_{k,k+1}c_{k+1}-h_{k+1}}{z'_i\,r_{k+1}}) \tag{21}$$

$$(D_x)_{ij}=-2z'_i\sum_{k=1}^{N}\frac{(y'_{k+1}-y'_k)(r_k+r_{k+1})}{r_k r_{k+1}\left[(r_k+r_{k+1})^2-l_{k,k+1}^2\right]} \tag{22}$$

$$(D_y)_{ij}=2z'_i\sum_{k=1}^{N}\frac{(x'_{k+1}-x'_k)(r_k+r_{k+1})}{r_k r_{k+1}\left[(r_k+r_{k+1})^2-l_{k,k+1}^2\right]} \tag{23}$$

$$c_k=(x'_k-x'_i)^2+z'^2_i \qquad h_k=(x'_k-x'_i)(y'_k-y'_i) \tag{24}$$

$$m_{k,k+1}=\frac{y'_{k+1}-y'_k}{x'_{k+1}-x'_k} \qquad r_k=\sqrt{c_k+(y'_k-y'_i)^2} \tag{25}$$

where (x'_i,y'_i,z'_i) is the position of field point, (x'_j,y'_j,z'_j) is the position of source point, and (x'_k,y'_k,z'_k) is the k-th corner point of the panel j. $N=3$ for a triangular panel on the hull surface, and $N=4$ for a four-nodes panel on the free surface. $l_{k,k+1}$ is the distance between k-th corner point and $(k+1)$-th corner point. In the local coordinate system (x',y',z'), the normal vector is assumed to point to the inside of the hull on the hull surface panel and upward on the free surface panel. When $i=j$, the integration in Eq. (21) is analytically performed giving $D_{ij}=2\pi$. More details about the integration of the coefficients can be found in [2, 7].

The same method is used to expand the perturbed velocity potential φ, and the hull surface boundary condition is similar to that of Eqs. (18), (19) and (20):

$$4\pi(\varphi)_i+\sum_{j=1}^{N_b+N_f}D_{ij}(\varphi)_j+\sum_{j=1}^{N_b+N_f}(D^{x'})_{ij}(\varphi_{x'})_j+\sum_{j=1}^{N_b+N_f}(D^{y'})_{ij}(\varphi_{y'})_j=0 \tag{26}$$

$$4\pi(\varphi_x)_i+\sum_{j=1}^{N_b}(D_x)_{ij}(\varphi)_j+\sum_{j=1}^{N_b}(D_x^{x'})_{ij}(\varphi_{x'})_j+\sum_{j=1}^{N_b}(D_x^{y'})_{ij}(\varphi_{y'})_j=0 \tag{27}$$

$$4\pi(\varphi_y)_i+\sum_{j=1}^{N_b}(D_y)_{ij}(\varphi)_j+\sum_{j=1}^{N_b}(D_y^{x'})_{ij}(\varphi_{x'})_j+\sum_{j=1}^{N_b}(D_y^{y'})_{ij}(\varphi_{y'})_j=0 \tag{28}$$

where $i=1,2,...,N_b$.

On the free surface, the boundary condition is:

$$4\pi(\varphi)_i+\sum_{j=1}^{N_b+N_f}D_{ij}(\varphi)_j+\sum_{j=1}^{N_b+N_f}(D^{x'})_{ij}(\varphi_{x'})_j+\sum_{j=1}^{N_b+N_f}(D^{y'})_{ij}(\varphi_{y'})_j=\sum_{j=1}^{N_f}S_{ij}(\varphi_{z'})_j \tag{29}$$

$$4\pi(\varphi_x)_i+\sum_{j=1}^{N_b+N_f}(D_x)_{ij}(\varphi)_j+\sum_{j=1}^{N_b+N_f}(D_x^{x'})_{ij}(\varphi_{x'})+\sum_{j=1}^{N_b+N_f}(D_x^{y'})_{ij}(\varphi_{y'})_j=\sum_{j=1}^{N_f}(S_x)_{ij}(\varphi_{z'})_j \tag{30}$$

$$4\pi(\varphi_y)_i+\sum_{j=1}^{N_b+N_f}(D_y)_{ij}(\varphi)_j+\sum_{j=1}^{N_b+N_f}(D_y^{x'})_{ij}(\varphi_{x'})_j+\sum_{j=1}^{N_b+N_f}(D_y^{y'})_{ij}(\varphi_{y'})_j=\sum_{j=1}^{N_f}(S_y)_{ij}(\varphi_{z'})_j \tag{31}$$

where $i=1,2,...,N_f$.

From Eqs. (29) to (31), the extra unknown number $\varphi_{z'}$ should be eliminated to complete the equation system. Hence, we transform the free surface condition as follows:

$$\varphi_{z'}=-\frac{1}{g}\phi_l^2\phi_{ll}-\frac{2}{g}\phi_{ll}\varphi_l-\frac{1}{g}\phi_l^2\varphi_{ll} \tag{32}$$

In the right side of Eqs. (32), the value of the first term is known, and the other two terms are unknown terms to be solved. We insert Eqs. (32) to Eqs. (29), (30) and (31). Before combining the terms with the same unknown number, the variables should be transformed into the same co-ordinate system by using the transition matrix:

$$\begin{bmatrix}(\varphi_x)_j\\(\varphi_y)_j\end{bmatrix}=\begin{bmatrix}a_1 & b_1\\a_2 & b_2\end{bmatrix}\begin{bmatrix}(\varphi_{x'})_j\\(\varphi_{y'})_j\end{bmatrix} \tag{33}$$

Through transformation of co-ordinates, φ_l and φ_{ll} in panel j can be expressed as:

$$(\varphi_l)_j = (\varphi_x)_j (l_x)_j + (\varphi_y)_m (l_y)_j$$
$$= [(a_1)_j (\varphi_{x'})_j + (b_1)_j (\varphi_{y'})_j](l_x)_j + [(a_2)_j (\varphi_{x'})_j + (b_2)_j (\varphi_{y'})_j](l_y)_j \quad (34)$$

$$(\varphi_{ll})_j = (l_x)_j \frac{\partial}{\partial x}[(\varphi_x)_j (l_x)_j + (\varphi_y)_j (l_y)_j] + (l_y)_j \frac{\partial}{\partial y}[(\varphi_x)_j (l_x)_j + (\varphi_y)_j (l_y)_j] \quad (35)$$
$$= (\varphi_{xx})_j (l_x^2)_j + 2(\varphi_{xy})_j (l_x l_y)_j + (\varphi_{yy})_j (l_y^2)_j$$

The second order derivatives φ_{xx}, φ_{xy} and φ_{yy} in Eqs. (35) can be expressed as:

$$\begin{cases} (\varphi_{xx})_j = [(\varphi_x)_L]_j [L_x]_j + [(\varphi_x)_H]_j [H_x]_j \\ (\varphi_{xy})_j = [(\varphi_x)_L]_j [L_y]_j + [(\varphi_x)_H]_j [H_y]_j \\ (\varphi_{yy})_j = [(\varphi_y)_L]_j [L_y]_j + [(\varphi_y)_H]_j [H_y]_j \end{cases} \quad (36)$$

where L and H is specified as the difference operator in the longitudinal direction and lateral direction, which is given in [21].

By inserting Eqs. (33) and (36) into Eqs. (35), φ_{ll} can be expressed by $\varphi_{x'}$ and $\varphi_{y'}$. Consequently, $\varphi_{z'}$ can also be expressed by $\varphi_{x'}$ and $\varphi_{y'}$. on inserting $\varphi_{z'}$ into Eqs. (29), (30) and (31), and combining the like terms. The perturbed velocity potential φ and its tangential derivatives $\varphi_{x'}$ and $\varphi_{y'}$ can be obtained by solving the simultaneous equation system consisted of Eqs. (26) to (31).

WAVE PROFILE, WAVE-MAKING RESISTANCE AND HULL GESTURE

When the velocity potential ϕ, φ and their tangential derivatives $\phi_{x'}$, $\phi_{y'}$, $\varphi_{x'}$, $\varphi_{y'}$ are obtained, we transform the velocity in control points to global coordinate system by using transformation matrix:

$$\begin{bmatrix} \phi_x \\ \phi_y \\ \phi_z \end{bmatrix} = [\boldsymbol{T}] \begin{bmatrix} \phi_{x'} \\ \phi_{y'} \\ 0 \end{bmatrix} \quad (37)$$

where T is the transformation matrix.

The velocity vector in control point of hull surface:

$$\boldsymbol{V} = \nabla\overline{\varphi} + \nabla\varphi - (\boldsymbol{U}\cdot\boldsymbol{n})\boldsymbol{n} \quad (38)$$

The velocity vector in control point of free surface:

$$V_x = U + \varphi_x - \frac{1}{4\pi}\sum_{j=1}^{N_b}(D_x)_{ij}(\overline{\varphi})_j - \frac{1}{4\pi}\sum_{j=1}^{N_b}(D_x^{x'})_{ij}(\overline{\varphi}_{x'})_j - \frac{1}{4\pi}\sum_{j=1}^{N_b}(D_x^{y'})_{ij}(\overline{\varphi}_{y'})_j - \frac{1}{4\pi}\sum_{j=1}^{N_b}(S_x)_{ij}(\boldsymbol{U}\cdot\boldsymbol{n}_j)$$
$$V_y = \varphi_y - \frac{1}{4\pi}\sum_{j=1}^{N_b}(D_y)_{ij}(\overline{\varphi})_j - \frac{1}{4\pi}\sum_{j=1}^{N_b}(D_y^{x'})_{ij}(\overline{\varphi}_{x'})_j - \frac{1}{4\pi}\sum_{j=1}^{N_b}(D_y^{y'})_{ij}(\overline{\varphi}_{y'})_j - \frac{1}{4\pi}\sum_{j=1}^{N_b}(S_y)_{ij}(\boldsymbol{U}\cdot\boldsymbol{n}_j) \quad (39)$$

The pressure coefficient of hull surface, coefficient of wave-making resistance and wave profile can be obtained by:

$$C_p = 1 - (\frac{\nabla\Phi}{U})^2 \quad (40)$$

$$C_w = \sum_{i=1}^{N_b} C_{p_i} n_{x_i} S_i \Big/ \sum_{i=1}^{N_b} S_i \quad (41)$$

$$C_{Fz} = \sum_{i=1}^{N_B} C_{p_i} n_{zi} S_i \Big/ \sum_{i=1}^{N_b} S_i \quad (42)$$

$$C_{Ny} = \sum_{i=1}^{N_B} C_{p_i} \left[(z_i - z_g) n_{xi} - (x_i - x_g) n_{zi} \right] S_i \Big/ \sum_{i=1}^{N_b} x_i S_i \quad (43)$$

$$\zeta = \frac{1}{2g}(|\boldsymbol{U}|^2 - |\boldsymbol{V}_i|^2) \quad (44)$$

where S_i is the wetted area of hull surface, x_i, z_i are the coordinates of i-th control point, x_g, z_g are the coordinates of ship gravity centre, n_{xi}, n_{zi} are the normal vectors of *i*-th panel.

The problem discussed in this paper is steady, but the hull gesture (i.e. its floating position against calm water line) will be obtained by iteration method. To this end, a time step Δt is used to calculate the change of trim and sinkage in the next step. After calculating the lifting force and trim moment, the hull position of the next step is obtained, and the hull surface under free surface will be re-meshed. The most part of the mesh can be used again, only the part near the waterline should be re-meshed:

$$S_{t+\Delta t} = S_t + \frac{F_z}{m}\Delta t \qquad T_{t+\Delta t} = T_t + \frac{N_y}{m}\Delta t \quad (45)$$

where m is the mass of ship, S_t and T_t are sinkage and trim in time step t, respectively. After performing iterations until the convergence condition ($F_z < \varepsilon, N_y < \varepsilon$) is satisfied, the wave-making resistance, hull sinkage and trim, and wave profile are obtained.

RESULTS AND DISCUSSION

In this section, the Wigley hull is used to test the convergence and difference schemes of the current method. Then, S60 and KVLCC2 models with the block coefficient of 0.6 and 0.8 , respectively, are simulated to validate the current method.

3.1 WIGLEY HULL

Wigley hull model is taken as an example, and different numerical methods and mesh schemes are used to discuss the convergence of the TEBEM and the effect of different parameters on the result. The Wigley hull model is define by the analytical formula as follows:

$$y = \frac{B}{2}(1-(\frac{x}{L/2})^2)(1-(\frac{z}{D})^2)$$

where L, B and D are the waterline length, breadth and depth of Wigley hull , respectively, and the main ship dimension ratios are $B/L = 0.1$, $D/L = 0.063$, and $C_b = 0.444$.

The mesh generation is similar to that given in [21], but, in this paper, every rectangular panel of hull surface is divided into two triangular panels. Ship hull is divided into 70 sections longitudinally and 5 sections vertically, so there are 70×12 panels on a half of the hull surface, which is shown in Fig. 1. Free surface panel mesh varies with the Froude number, and every wavelength is divided into 20 sections in the longitudinal direction. The length of panels before stem and behind stern are enlarged in a ratio of 1.06, and , similarly, their breadth values. The length of the panels before stem, behind stern and their breadth are kept greater than $1L$, $1.5L$ and $1L$, respectively. The free surface is discretized into the mesh of 30×84 when F_n is 0.25. Fig. 2 shows the free surface panel arrangement at F_n=0.25.

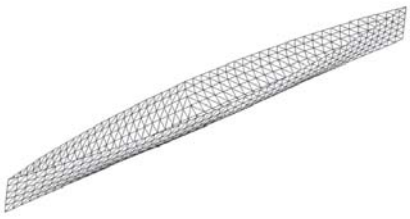

Fig. 1. Panel arrangement of Wigley hull model.

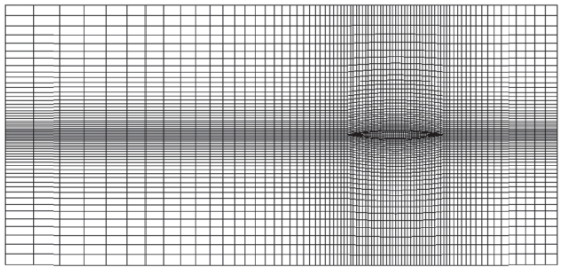

Fig. 2. Free surface panel arrangement at F_n=0.25.

The current numerical method is applied to calculate the hull gesture, wave profile and wave-making resistance of Wigley model, The convergence and difference schemes are discussed.

The two-point, three-point and four-point difference operators are used for calculation to discuss the effect of various difference operations on the results. In Fig. 3, the wave-making resistance with free sinkage and trim obtained from three kinds of difference operators are compared with the experimental results carried out by Ship Research Institute [8]. It shows that the four-point difference operator will lead to oscillation of the result at some Froude numbers. The result obtained from the three-point difference operator is accurate in a wide range of Froude numbers. Consequently, the three-point operator is used as the most stable difference scheme for the TEBEM method at a wide range of Froude numbers.

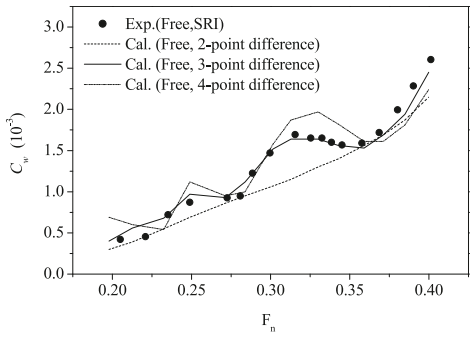

Fig. 3. Wave-making resistance of Wigley hull by using various difference operators (Free).

The convergence of the TEBEM is also tested. The hull surface is discretized into the mesh of 50×8, 70×10 and 90×12 respectively. The wave-making resistance, sinkage and trim calculated with different mesh schemes are compared in Fig. 4, Fig. 5 and Fig. 6, It shows that the results for wave-making resistance obtained from the mesh of 50×8 and 70×10 are almost the same with each other, and calculations of trim and sinkage converge faster than wave-making resistance. Hence, for the TEBEM method, discretizing the hull surface into triangular grids may be efficient enough for numerical simulation. Compared with source panel, the dipole is more sensitive to the gap between two panels, when the four points of panel is projected to the same plane, but with the use of the triangular grid this problem can solved for dipole.

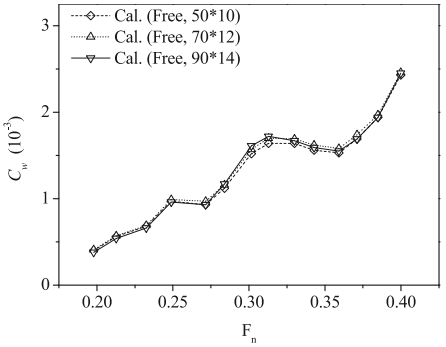

Fig. 4. Calculated wave-making resistance by using different mesh schemes (Free).

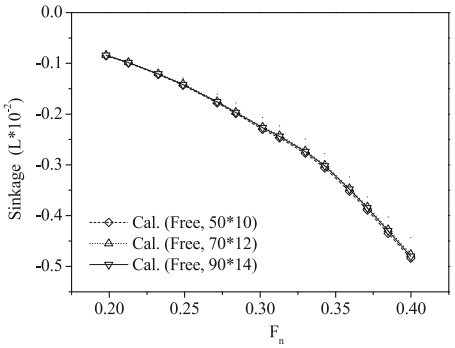

Fig. 5. Calculated sinkage by using different mesh schemes (Free).

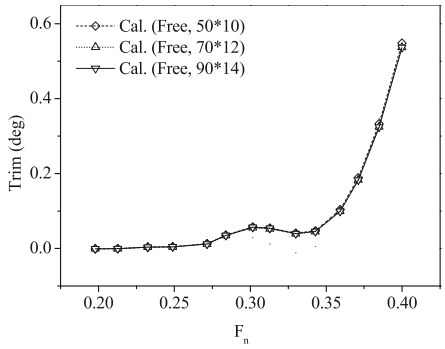

Fig. 6. Calculated trim by using different mesh schemes (Free).

3.2 SERIES 60 MODEL

The main characteristic particulars of Series 60 are as follows: $C_b = 0.6$, $B/L = 0.133$ and $D/L = 0.054$. Hull surface is discretized into 74×20 mesh. On the free surface, 30 panels per wavelength are kept in the direction of x-axis, and the width of the first panel near the ship is $0.018L$. The enlarging rates in the ship longitudinal and lateral direction are the same, equal to 1.06. The free surface is discretized into 136×30 mesh when Froude number is 0.316. Fig. 7 shows the panel arrangement of Series 60 model.

(a)

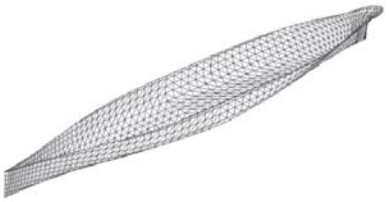

(b)

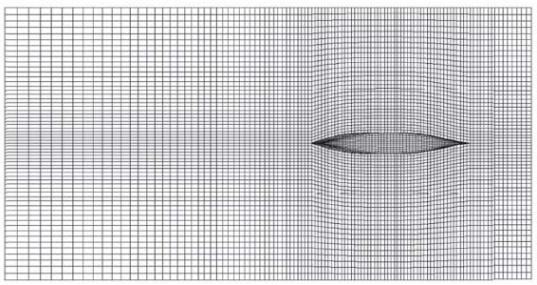

Fig. 7. Panel arrangement of Series 60 model : (a) Panel arrangement of hull surface, (b) Panel arrangement of free surface.

The fixed model without sinkage and trim is calculated first, and the calculated wave-making resistance and wave profile are compared with the experimental result. Fig. 8 shows the comparison of the calculated wave-making resistance with the results of the experiment carried out by Ishikawajima-Harima Heavy Industries Co., Ltd. and University of Tokyo [8], respectively.

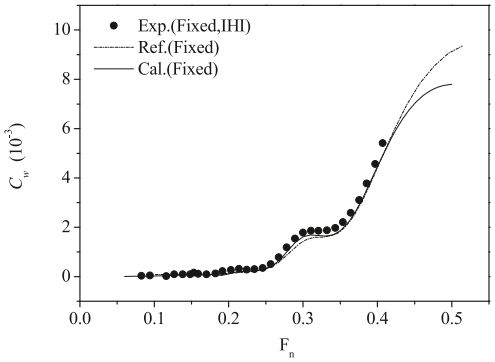

Fig. 8. Wave-making resistance of Series 60 model (Fixed)

In Fig. 9, the calculated wave profile of Series 60 model with fixed sinkage and trim is compared with the experimental result and the result presented in [21] achieved by using the improved Dawson's method; the experiment was carried out by Ship Research Institute [8]. The calculated result is in a good agreement with the experimental result at different Froude numbers. It shows that the accuracy of the wave profile along ship is improved, and almost all the difference appears in the first crest of the wave profile, but the difference is relatively smaller for different Froude numbers..

(a)

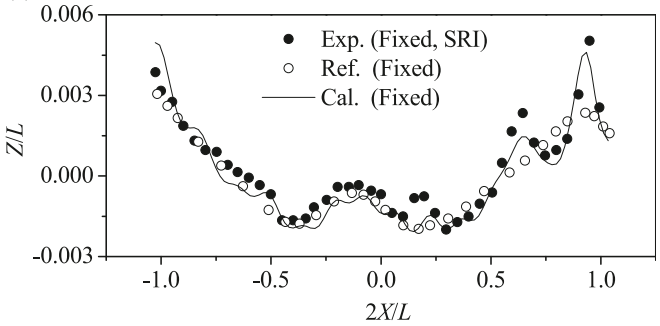

(b)

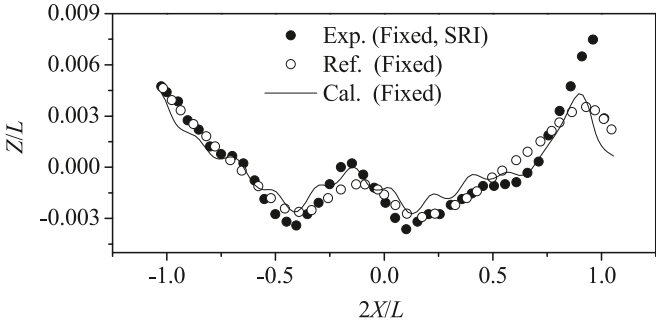

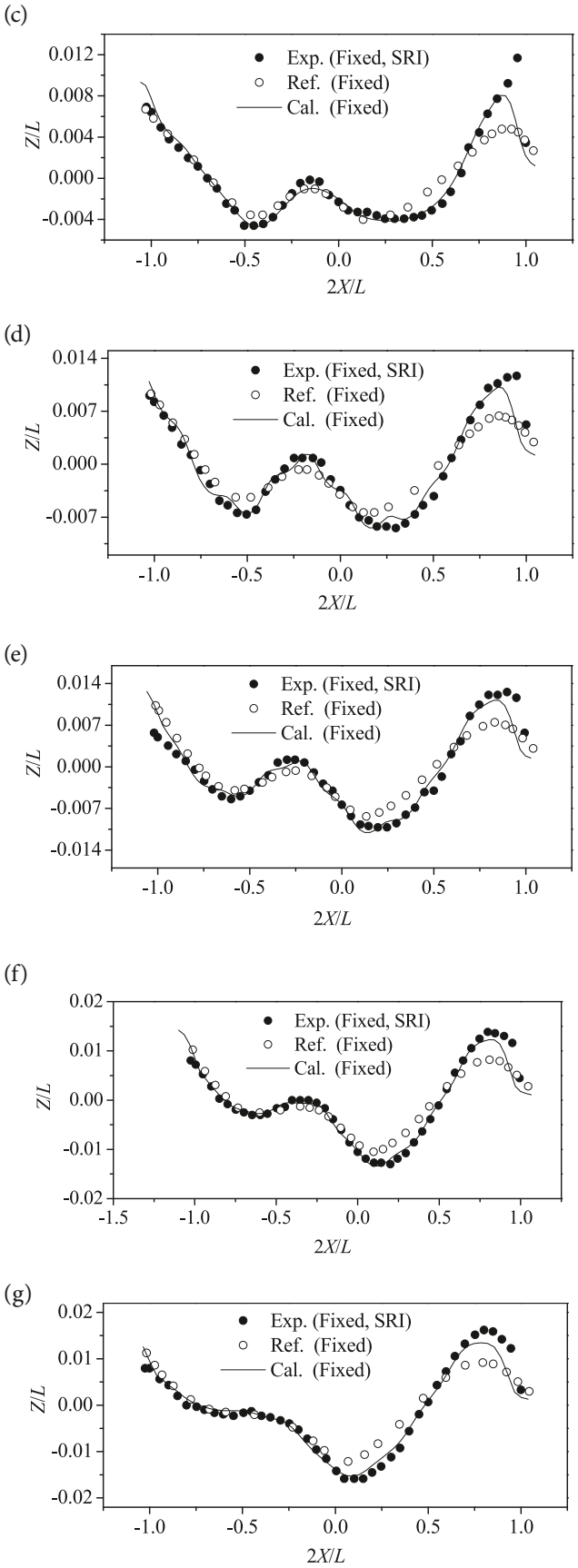

Fig. 9. Wave profile of Series 60 model at different F_n (Fixed). (a) wave profile at F_n=0.18 (b) wave profile at F_n=0.22, (c) wave profile at F_n=0.25, (d) wave profile at F_n=0.28, (e) wave profile at F_n=0.30, (f) wave profile at F_n=0.32, (g) wave profile at F_n=0.34.

To test the propagation and dissipation of waves, the calculated and experimental wave profiles in different longitudinally placed cross-sections are compared with each other (F_n=0.316). The experiment was carried out by Iowa Institute of Hydraulic Research [23]. Fig. 10 shows that only at the cross-section y=0.2067L a little phase difference appears.

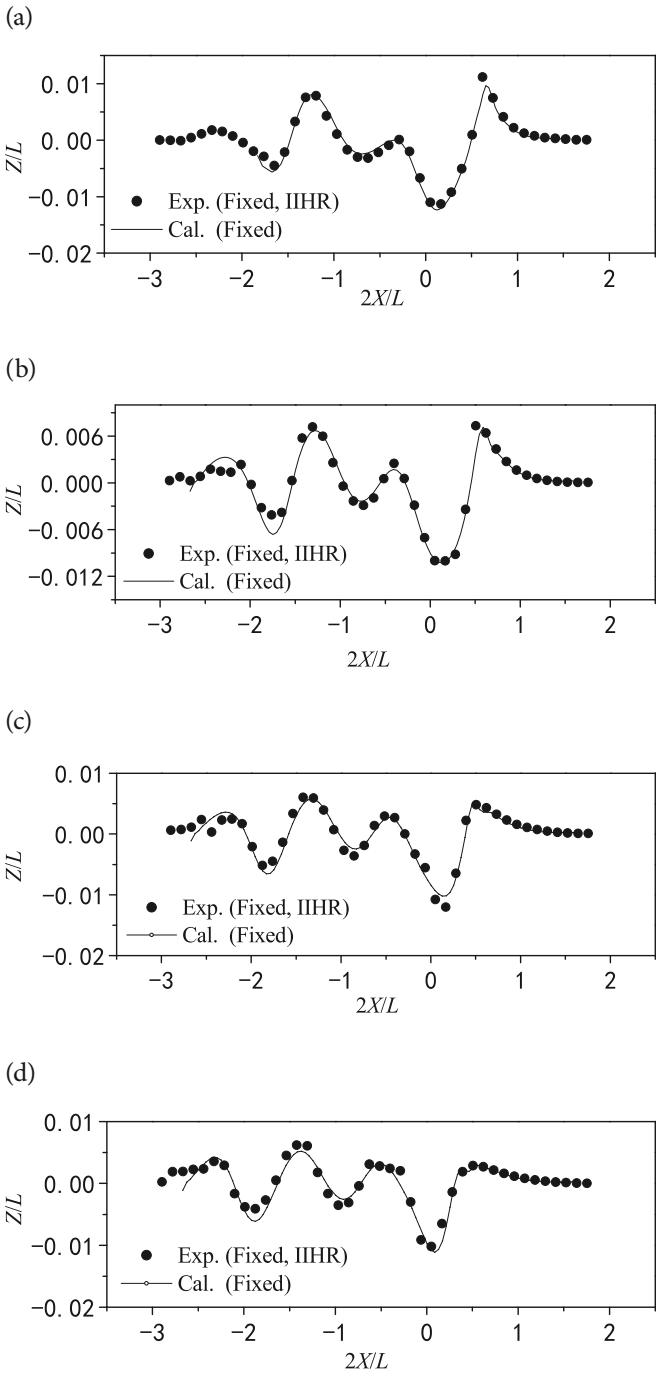

(e)

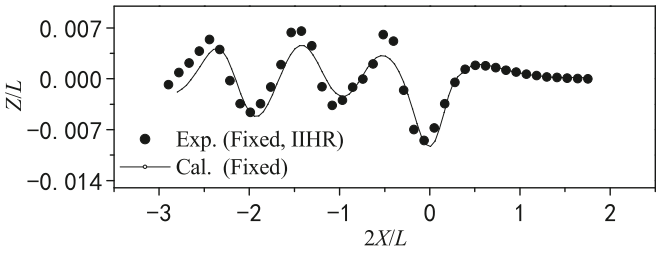

Fig. 10. Wave profile of Series 60 model in different longitudinally placed cross-sections at $F_n = 0.316$ *(Fixed). (a) wave profile at* $y = 0.1083L$, *(b) wave profile at* $y = 0.1411L$, *(c) wave profile at* $y = 0.1739L$, *(d) wave profile at* $y = 0.2067L$.

Numerical simulation of Series 60 model with free sinkage and trim was also carried out. The calculated wave-making resistance and hull sinkage and trim are compared with the experimental result in Fig. 11, 12 and 13. All the experiment was carried out by Iowa Institute of Hydraulic Research [23].

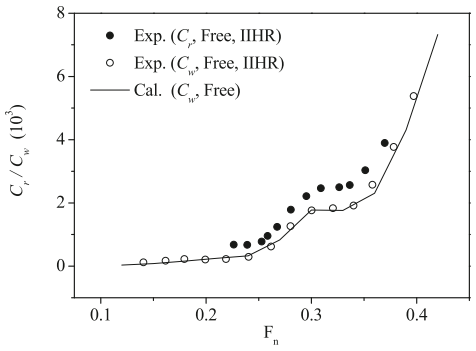

Fig. 11. Wave-making resistance of Series 60 model (Free).

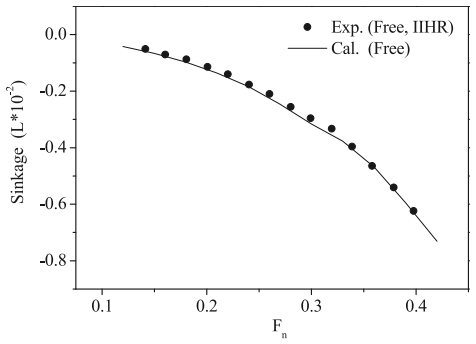

Fig. 12. Sinkage of Series 60 model (Free).

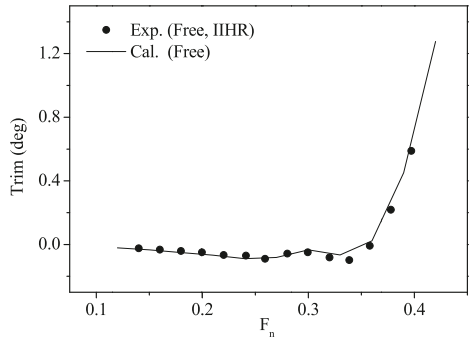

Fig. 13. Trim of Series 60 model (Free).

Fig. 14 shows the wave pattern of Series 60 model at different Froude numbers.

(a)

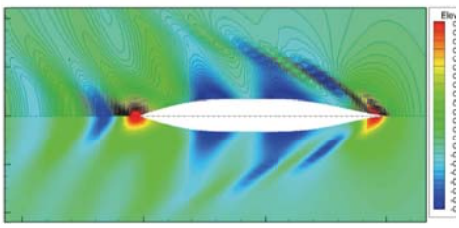

(b)

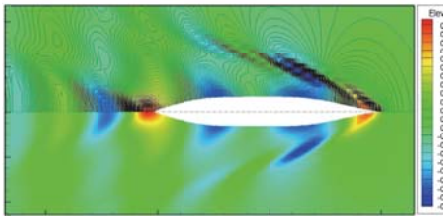

(c)

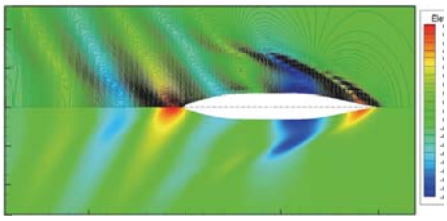

(d)

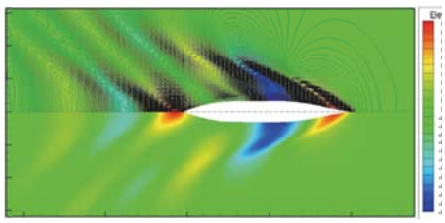

(e)

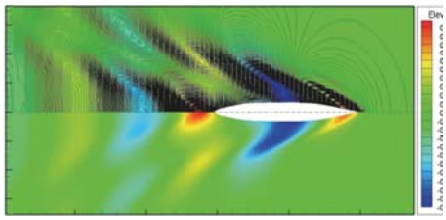

Fig. 14. Wave pattern of Series 60 model at different F_n *(Free). (a) wave pattern at* F_n=0.22, *(b) wave pattern at* F_n=0.26, *(c) wave pattern at* F_n=0.30, *(d) wave pattern at* F_n=0.34, *(e) wave pattern at* F_n=0.38.

KVLCC2 MODEL

KVLCC2 models are taken as examples to validate application of the numerical method based on the TEBEM

for full form ship. Compared with the series 60 models, the simulation of flow around a full form ship, such as KVLCC2 one, is relatively more complicated. In the reference [14] about the prediction of flow around full form ship, the domain of free surface behind the stern is neglected to avoid the oscillation of wave-making. In this section, both the free and fixed KVLCC2 model was calculated. To compare with the experimental and CFD results, when simulating the fixed and free model, the simplified rudder which is of the same size as that used in the Gothenburg Workshop 2010 [10], is included. The main characteristic particulars of KVLCC2 model are as follows: block coefficient $C_b = 0.8$, $B/L = 0.178$ and $D/L = 0.064$.

The fixed KVLCC2 model with and without rudder is calculated at Fn=0.142 first to test the accuracy of wave profile. Because a part of the ship hull is parallel body and its block coefficient is very large, a triangular mesh is applied to make the hull surface smoother. Fig. 15 shows the panel arrangement on hull surface and free surface.

(a)

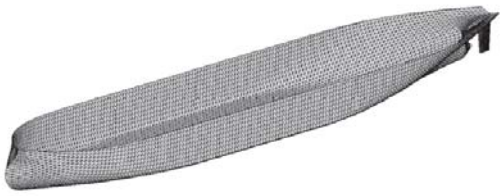

(b)

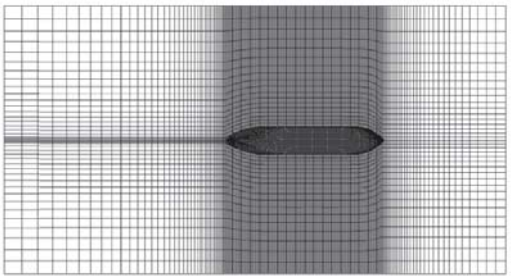

Fig. 15. Panel arrangement of KVLCC2 model with rudder. (a) Panel arrangement on hull surface, (b) Panel arrangement on free surface at F_n=0.142.

The mesh generation is the same as for Wigley hull, the domain size is $3.5L \times 1.0L$, where the length before stem is $1.0L$, the length behind stern is $1.5L$, and the width of the domain is $1.0L$ [14], and the free surface is divided into 25×297 panels at $Fn = 0.142$. Because KVLCC2 model is a full form ship, three sets of hull surface mesh schemes are used to test the calculation convergence.

Based on Fig. 16, Fig. 17 and Fig. 18, the result shows that the 4596 cell mesh is fine enough for calculating hull gesture and wave profile as the relative difference of the sinkage and trim results calculated with the use of 4596 panels and 7578 panels is lower than 1%. For the numerical simulation of full form ship by the TEBEM it is enough to divide half of the hull surface into 4596 panels, but compared with series 60 form, a greater number of cells is necessary for full form ship, especially for the area of stem and stern. Based on Fig. 16, we can also make sure ourselves that for the full form ship, the radiation condition suggested by Nakos [13] is well satisfied on the free surface before the bow, and the wave elevation goes to zero when, $2X/L \to 2$.

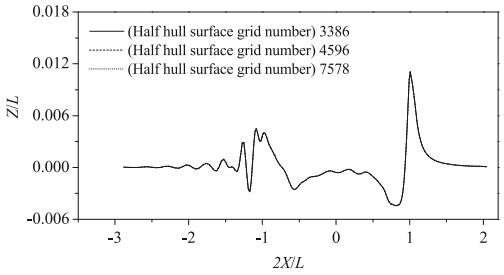

Fig. 16. Computed wave profile along the hull by using different hull surface meshes at F_n=0.15 *(Free model).*

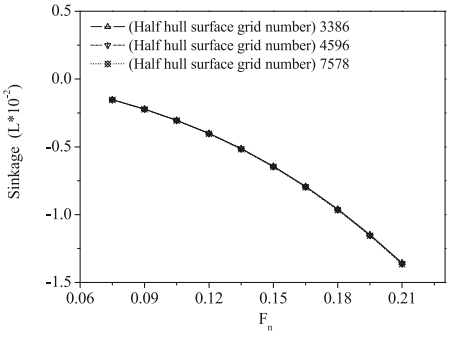

Fig. 17. Computed sinkage by using different mesh schemes (Free model)

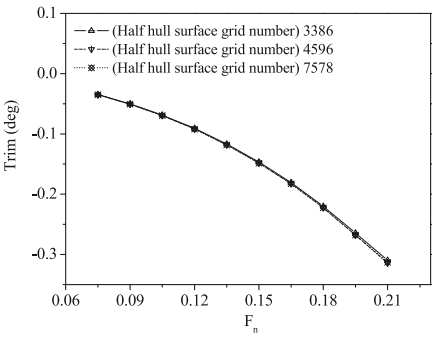

Fig. 18. Computed trim by using different mesh schemes (Free model)

In Fig. 19, the calculated wave profiles of the fixed model at different cross-sections are compared with the experimental results and CFD results; all the data come from the report of Gothenburg Workshop 2010 [14]. Fig. 19 (a) shows that the computed wave profile for the model without rudder is in a good agreement with the experimental results, and the first peak and hollow values differ by 4.5% and 9.1%, respectively, from their experimental results. The computed pressure coefficient of the hull surface is shown in Fig. 20(a), and the Fig. 20(b) presents the comparison between the computed results and CFD ones [10]. Fig. 21shows the contour of wave elevation.

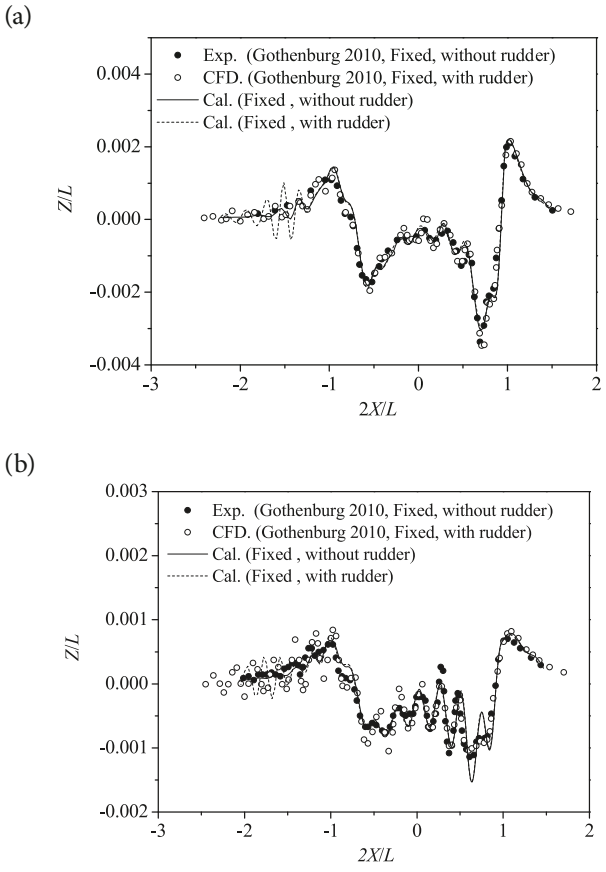

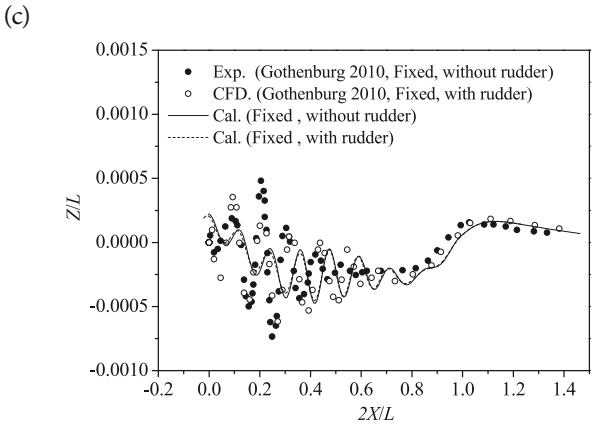

Fig. 19. Wave profile of KVLCC2 model in different longitudinally situated cross-sections at F_n=0.142 (Fixed). (a) wave profile at y=0.096L , (b) wave profile at y=0.158L (c) wave profile at y=0.299L .

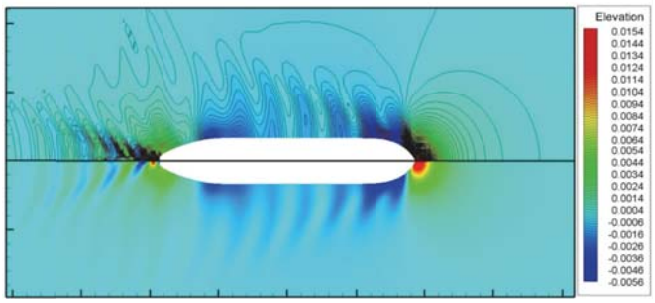

Fig. 21. Wave pattern for KVLCC2 model at F_n=0.142 (Fixed, without rudder).

In Fig. 19(b), some oscillations of the wave-making appear behind stern for both the computed and CFD result, which reflects the effect of rudder on wave pattern. From Fig. 19(c) it also results that the wave profile computed by the TEBEM method damps faster than in case of experimental and CFD

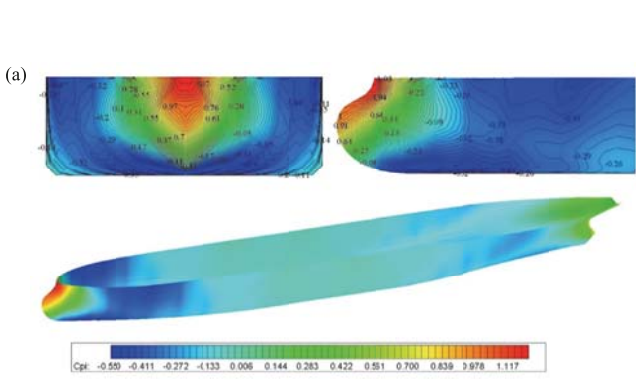

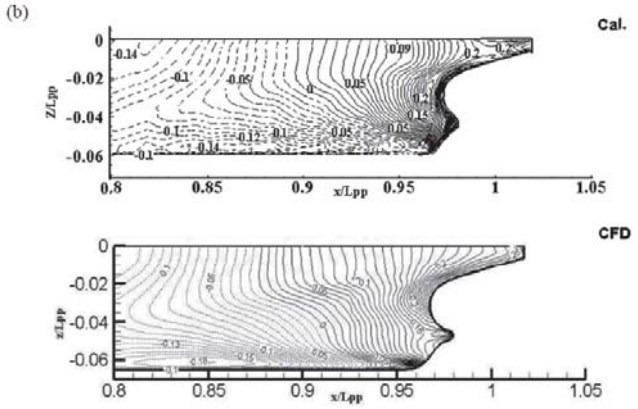

Fig. 20. Pressure coefficient field on KVLCC2 hull surface at F_n=0.142 (Fixed, without rudder), (a) computed result, (b) comparison with CFD result [10].

results, when a considered field point is distant far away from the hull surface, and both the results obtained from CFD and TEBEM calculations show a phase difference compared with the experimental result. The comparison given in Fig. 20(b) shows that the tendency of the pressure gradient lines obtained by means of the current method is similar to that of the CFD result. But the negative pressure area calculated by using the current method is larger than that by CFD, it is probably because the viscous effect is neglected, and the streamline separation by an adverse pressure gradient in this area may also affect the pressure distribution. Fig. 21 shows that, though the wave profile in different sections is in a good agreement with the experimental result, some short waves, especially the break waves generated by the bow with large curvature, are not covered by the current methods,

The KVLCC2 model with free trim and sinkage is simulated at different Froude numbers, and the results are compared with the experimental and CFD results taken from the report of Gothenburg Workshop 2010 [14], which is shown in Fig. 22 and 23. To keep the computed model the same as that used for the experiment, the rudder is included in the free model. Fig. 24 shows the wave pattern of free KVLCC2 model with rudder for three different Froude numbers.

Fig. 22. Sinkage of KVLCC2 model (Free, with rudder).

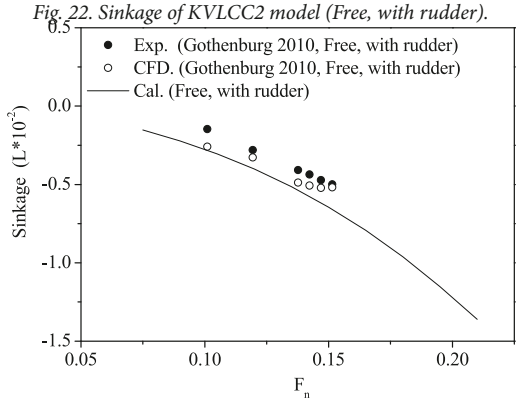

Fig. 23. Trim of KVLCC2 model (Free, with rudder).

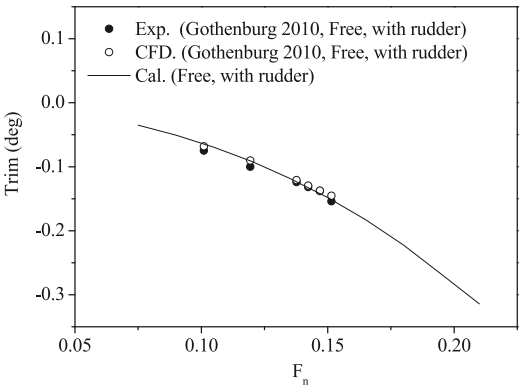

(a)
(b)
(c)

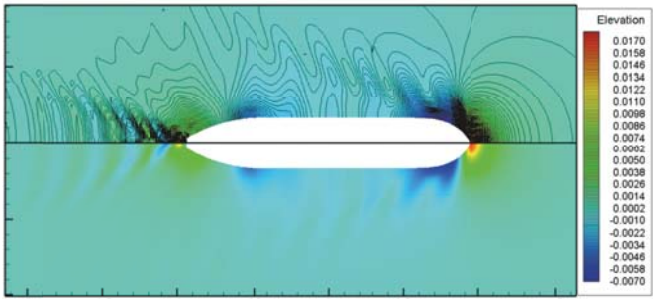

Fig. 24. Wave pattern for KVLCC2 model (Free, with rudder), (a) F_n=0.15 (b) F_n=0.15 (c) F_n=0.21.

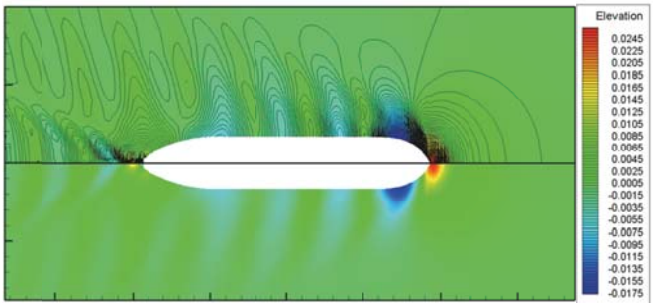

Based on the simulation of KVLCC2 model with free trim

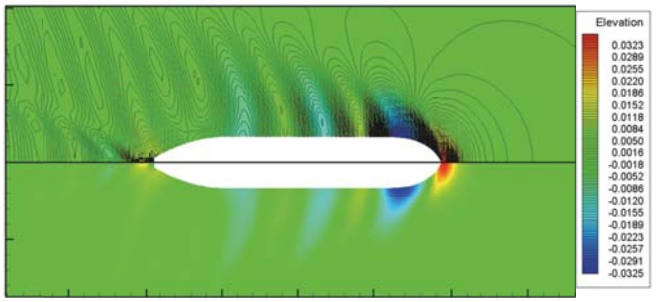

and sinkage, Fig. 22 and Fig. 23 shows that the computed trim of full form ship is in a good agreement with the experimental result, and the sinkage is larger than that from both the experimental and CFD results. The wave contour of Fig. 24 shows that the wave for full form ship computed by using the current method is stable at different Froude numbers without excluding the free surface mesh behind the transom stern, and the wave generated by both the bulbous bow and transom stern can be successfully determined without oscillation, which is very important for hull form optimization, because a comparison of the wave profiles is a traditional method to judge the resistance performance.

CONCLUSIONS

The TEBEM combined with the simplified free surface condition is presented in this paper for the prediction of the wave-making resistance, hull gesture and wave profile of

different hull forms, and the calculated results for different hull forms are compared with the experimental results. The following conclusions are drawn from this paper:

When the TEBEM is applied the boundary condition of tangential velocity is exerted at every control point and calculated directly. The computed results show that the TEBEM method is efficient in predicting the wave-making resistance, hull gesture and wave pattern for different hull forms, and accurate wave profile and hull response can be obtained even for a full form ship with large block coefficient.

The calculations based on different schemes of hull surface discretization proved that the calculation with the use of the current method converges well, whereas the mesh scheme has a little effect on the computed results.

Because the TEBEM leads to the three times greater amount of the known numbers than the traditional method, the computing time for the TEBEM is relatively greater than in case of the traditional method.

For the full form ship, some short waves are not contained in the computed wave pattern, and the negative pressure area of hull surface is relatively larger than that resulting from the CFD calculations, which leads to that the sinkage computed by using the current method is a little larger. This is perhaps limited by the non-viscosity and the linear free surface condition, therefore in the future work the TEBEM method will be applied to a nonlinear method.

BIBLIOGRAPHY

1. Chen J.K., Duan W.Y., Zhao B.B., Ma Q.W. : *Time domain hybrid TEBEM for 3D hydrodynamics of ship with large flare at forward speed.* The 32nd International Workshop on Water Waves and Floating Bodies, Dalian, China, , 2017, pp. 23-26.

2. Dai, Y. : *Potential flow theory of ship motions in waves*. National Defense Industry Publication, Beijing, , 2008. 11-33.

3. Dawson C.W.: A practical computer method for solving ship-wave problems. *In: Proceedings of Second International Conference on Numerical Ship Hydrodynamics*, pp. 30-38.

4. Doctors L.J., 2006. *A numerical study of the resistance of transom-stern monohulls.* In: Fifth International Conference on High-Performance Marine Vehicles, 1977, pp. 1-14.

5. Doctors L.J., Macfarlane G.J., Young R. : *A study of transom-stern ventilation*. In: International Shipbuilding Progress, 54, 2007, pp. 145-163.

6. Duan W.Y. : *Taylor expansion boundary element method for floating body hydrodynamics*. In: 27th International Workshop on Water Waves and Floating Bodies, 2012. Copenhagen, Danmark.

7. Duan W.Y., Chen, J.K., Zhao, B.B. : *Second-order Taylor expansion boundary element method for the second-order wave radiation problem*. Applied Ocean Research, 52, 2015, pp. 12-26.

8. IHI, SRI, U. of Tokyo and Yokohama N.U. : *Cooperative experiments on Wigley parabolic models in Japan*, 1983.

9. Guha A., Falzaranoa J. : *Application of multi-objective genetic algorithm in ship hull optimization*. Ocean System Engineering, Vol. 5, No. 2 (2015) , pp. 91-107.

10. Larsson L., Stern F., Visonneau M.: *A workshop on numerical ship hydrodynamics*. Gothenburg, Sweden, 2010.

11. Lu Y., Chang X., Hu A.K.: *A hydrodynamic optimization design methodology for a ship bulbous bow under multiple operating conditions*. Engineering Applications of Computational Fluid Mechanics, Vol. 10, 2016, No. 1, pp. 330–345.

12. Minchev A., Schmidt M., Schnack S. : *Contemporary bulk carrier design to meet IMO EEDI requirements*. Third International Symposium on Marine Propulsors, Launceston, Tasmania, 2013.

13. Nakos, D. E.: *Ship wave patterns and motions by a three dimensional Rankine panel method*. Massachusetts Institute of Technology, 1990.

14. Peng H., Ni S., Qiu W.: *Wave pattern and resistance prediction for ships of full form*. Ocean Engineering, 87, 2014 , pp. 162-173.

15. Raven H.C. :. *Nonlinear ship wave calculations using the rapid method*. In: Sixth International Conference on Numerical Ship Hydrodynamics, Iowa City, 1994

16. Raven H.C.: *A solution method for the nonlinear ship wave resistance problem*. A Dissertation for the Degree of Doctor., Delft University of Technology, 1996.

17. Sherbaz S.: *Ship Trim Optimization for Reducing Resistance by CFD Simulations*. A Dissertation for the Degree of Doctor, Harbin Engineering University, 2014.

18. Sun J.L., Tu H.W., Chen Y.N., Xie D., Zhou J.J.: *A study on trim optimization for a container ship based on effects due to resistance. Journal of Ship Research*, Vol. 60, 2016, No. 1, pp. 30–47

19. Tarafder M.S., Alia M.T., Nizamb M.S. : *Numerical prediction of wave-making resistance of pentamaran in unbounded water using a surface panel method.* Procedia Engineering, 56, 2013, pp. 287-296.

20. Takeshi H., Hino T., Hinatsu M., Tsukada Y., Fujisawa J.: *ITTC Cooperative Experiments on a Series 60 Model at Ship Research Institute-Flow Measurements and Resistance Test* , 1987

21. Tarafder M.S., Suzuki K. : *Numerical calculation of free-surface potential flow around a ship using the modified Rankine source panel method*. Ocean Engineering, 35, 2008, pp. 536-544.

22. Tarafder M.S., Suzuki K.: *Wave-making resistance of a catamaran hull in shallow water using a potential-based panel method*. Journal of Ship Research, 52(1), 2008, pp. 16-29.

23. Toda Y., Stern F., Longo J. : *Mean-flow measurements in the boundary layer and wake and wave field of a Series 60 CB=0.6 ship model for Froude Numbers 0.16 and 0.316*. IIHR Report, No. 352, 1991.

24. Zhang B.J. *The optimization of the hull form with the minimum wave making resistance based on Rankine source method*. Journal of hydrodynamics, 21(2) , 2009, pp. 277-284.

25. Zhang B.J., Miao A.: *The design of a hull form with the minimum total resistance.* Journal of Marine Science and Technology, 23(5) , 2015, pp. 591-597

26. Zhang B.J., Miao A. : *Research on design method of the full form ship with minimum thrust deduction factor*, China Ocean Eng., 29(2), 2015, pp. 301-310

CONTACT WITH THE AUTHORS

Yunbo Li
e-mail: yunboz@163.com

College of Ocean Science and Engineering of SMU,
Shanghai Maritime University
Shanghai
CHINA